Current Biology 23, 362–371, March 4, 2013 ©2013 Elsevier Ltd All rights reserved http://dx.doi.org/10.1016/j.cub.2013.01.045

Article

Moderation of *Arabidopsis* Root Stemness by CLAVATA1 and ARABIDOPSIS CRINKLY4 Receptor Kinase Complexes

Yvonne Stahl,[1,*] Stephanie Grabowski,[2] Andrea Bleckmann,[1,4] Ralf Kühnemuth,[2] Stefanie Weidtkamp-Peters,[3] Karine Gustavo Pinto,[1] Gwendolyn K. Kirschner,[1] Julia B. Schmid,[1] René H. Wink,[1] Adrian Hülsewede,[1] Suren Felekyan,[2] Claus A.M. Seidel,[2] and Rüdiger Simon[1]

[1]Institute of Developmental Genetics
[2]Institute for Molecular Physical Chemistry
[3]Center for Advanced Imaging
Heinrich Heine University, 40225 Düsseldorf, Germany

Summary

Background: The root system of higher plants originates from the activity of a root meristem, which comprises a group of highly specialized and long-lasting stem cells. Their maintenance and number is controlled by the quiescent center (QC) cells and by feedback signaling from differentiated cells. Root meristems may have evolved from structurally distinct shoot meristems; however, no common player acting in stemness control has been found so far.

Results: We show that CLAVATA1 (CLV1), a key receptor kinase in shoot stemness maintenance, performs a similar but distinct role in root meristems. We report that CLV1 is signaling, activated by the peptide ligand CLAVATA3/EMBRYO SURROUNDING REGION40 (CLE40), together with the receptor kinase ARABIDOPSIS CRINKLY4 (ACR4) to restrict root stemness. Both CLV1 and ACR4 overlap in their expression domains in the distal root meristem and localize to the plasma membrane (PM) and plasmodesmata (PDs), where ACR4 preferentially accumulates. Using multiparameter fluorescence image spectroscopy (MFIS), we show that CLV1 and ACR4 can form homo- and heteromeric complexes that differ in their composition depending on their subcellular localization.

Conclusions: We hypothesize that these homo- and heteromeric complexes may differentially regulate distal root meristem maintenance. We conclude that essential components of the ancestral shoot stemness regulatory system also act in the root and that the specific interaction of CLV1 with ACR4 serves to moderate and control stemness homeostasis in the root meristem. The structural differences between these two meristem types may have necessitated this recruitment of ACR4 for signaling by CLV1.

Introduction

The shoot and root meristems of higher plants maintain groups of stem cells that are required to provide new cells for organ production and for tissue differentiation [1]. In the shoot, the size of the entire stem cell population is controlled by negative feedback signaling with underlying cells that form the organizing center (OC). In *Arabidopsis thaliana*, the OC expresses the mobile homeodomain transcription factor WUSCHEL (WUS) [2, 3]. Stem cells in turn secrete the CLAVATA3 (CLV3) peptide that is perceived by the plasma membrane localized leucine-rich repeat (LRR) receptor kinase CLV1 [4–6], or through a parallel pathway comprising the LRR receptor protein CLAVATA2 (CLV2) and the receptor-like kinase CORYNE (CRN) to restrict *WUS* expression [7, 8], thereby achieving homeostasis of the stem cell population.

The architecture of the root stem cell niche is clearly distinct from the shoot system. Here, four cells of the mitotically silent quiescent center (QC) maintain the adjacent single layer of dedicated stem cells that each gives rise to a restricted number of cell types. QC cells express the WUSCHEL-RELATED HOMEOBOX5 (WOX5) protein, which maintains the undifferentiated status, or stemness, in abutting cells [9, 10]. A feedback mechanism, similar to the CLV pathway operating in the shoot, has been postulated to regulate the fate of columella stem cells (CSCs), which form cell layers immediately distal to the QC. Here, the CLV3 homolog CLE40 (CLAVATA3/EMBRYO SURROUNDING REGION40) acts as a signal from their differentiated descendants, the columella cells (CCs), to restrict *WOX5* expression [11, 12].

In contrast to the shoot system, feedback regulation in the root operates via the non-LRR receptor kinase ARABIDOPSIS CRINKLY4 (ACR4), which was previously shown to control formative cell divisions in lateral roots and epidermal cell layer integrity [13, 14]. Thus, regulation of stemness in root and shoot meristems employs similar but also distinct molecular mechanisms. We now asked whether the receptors controlling the shoot stem cell population also act to control overall root meristem maintenance. Both CLV2 and CRN are expressed in roots, but mutants are not affected in root stem cell regulation [8, 15, 16]. In phylogenetic terms, CLV2 and CRN have evolved recently in vascular plants, whereas CLV1 orthologs are already present in nonseed plants such as mosses that lack a root meristem [17]. Here we show that CLV1 can serve as the central hub that can perceive CLE signals to control stem cell number in both root and shoot meristems. We applied multiparameter fluorescence image spectroscopy (MFIS) as a novel two-dimensional assay based on Förster resonance energy transfer (FRET) to detect homo- and heteromerization of GFP-fused proteins in planta with high spatial resolution. Thereby, we could show that CLV1 and ACR4 can form different homo- and heteromeric complexes depending on their intracellular localization.

Results

CLV1 and ACR4 Are Expressed and Signal in the Distal Root Meristem

We first tested whether CLV1 contributes to stemness regulation in the *Arabidopsis* root system and generated transgenic plants expressing a functional CLV1-GFP fusion from the *CLV1* promoter that rescued the *clv1* mutant shoot phenotypes (see the Experimental Procedures for details). We found CLV1 expression in the two cell layers (D1 and D2) immediately distal to the QC, in epidermis/lateral root cap initials, and with

[4]Present address: Institute of Cell Biology and Plant Physiology, University of Regensburg, 93053 Regensburg, Germany
*Correspondence: yvonne.stahl@hhu.de

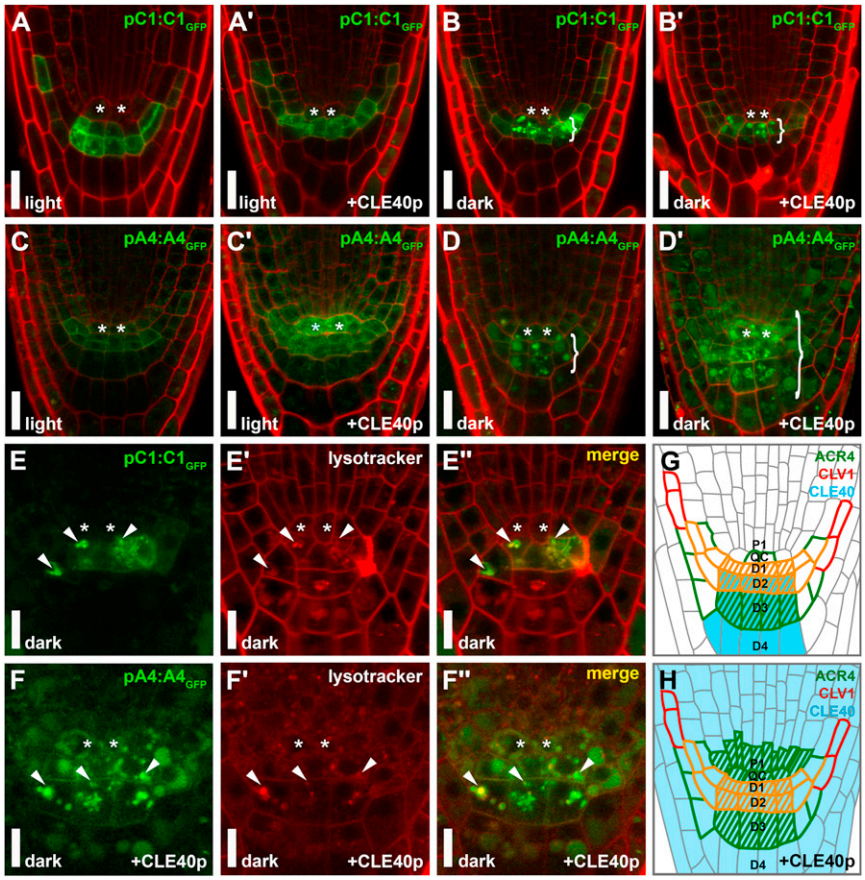

Figure 1. Expression Domains and Signaling Overlap of CLV1 and ACR4 in the Distal Root Meristem

(A–D′) *pCLV1:CLV1-GFP* (A–B′) and *pACR4:ACR4-GFP* (C–D′) reporter lines were analyzed in 5 days after germination roots grown on media without (A, B, C, and D) or with (A′, B′, C′, and D′) 200 nM CLE40p. Roots were either grown in the light (A, A′, C, and C′) or incubated in the dark (B, B′, D, and D′) for 24 hr prior to imaging. Asterisks indicate QC positions. Braces indicate the positions of the strong GFP signals in vacuolar compartments after dark incubation (B, B′, D, and D′). The pictures show representatives of 32–48 root tips analyzed from two to five biological replicates.

(E–E″) Colocalization of *pCLV1:CLV1-GFP* roots after dark incubation with LysoTracker Red.

(F–F″) Colocalization of *pACR4:ACR4-GFP* roots grown on media with 200 nM CLE40p after dark incubation with LysoTracker Red.

Scale bars represent 20 μm in (A)–(D′) and 10 μm in (E)–(F″).

(G and H) Schematic representation of expression (outlines and filled cells) and signaling (shaded area) of ACR4 (green), CLV1 (red), and CLE40 (light blue) observed without (G) and with (H) CLE40p treatment as observed in (A)–(D′). Overlap of ACR4 and CLV1 expression and/or signaling is depicted in orange.

C1, CLAVATA1; A4, ACR4. See also Figure S1 and Table S1.

variable expression levels in cells of the lateral root cap (Figures 1A and 1G). CLV1-GFP localized to the plasma membrane (PM) and also to small, mobile vesicles, which represent post-Golgi or endocytic vesicles, indicating active turnover of the protein [4]. In the shoot, binding of the CLV3 peptide ligand induces removal of CLV1 from the PM and trafficking to lytic vacuoles [4], whereas CLV1 remains mostly PM localized in the absence of the ligand. In the acidic lytic vacuole, the pH-sensitive GFP fluorescence cannot be detected, unless plants are dark-incubated for several hours to increase the vacuolar pH [4, 18]. After incubating *Arabidopsis* roots in the dark for 24 hr, we uncovered strong CLV1-GFP fluorescence in vesicular compartments of cells in the D1 and D2 position of the root meristem (Figure 1B). Using LysoTracker, we identified the majority of these vesicular compartments as lytic vacuoles (Figures 1B and 1E–1E″). The cells at the D1 to D4 position normally express the CLV3-related ligand CLE40 [11], which was shown to bind CLV1 receptor in in vitro studies [19]. This indicated that in D1 and D2 cells, CLV1 is activated, internalized, and removed to the lytic vacuole upon binding of CLE40. We next asked whether increasing CLE40 levels by the addition of synthetic CLE40 peptide (CLE40p) to the whole root affects CLV1-GFP expression or internalization. Dark incubation revealed that CLV1-GFP PM localization was reduced, but overall CLV1 expression levels were not altered (Figures 1B and 1B′ and Table S1 available online).

The expression pattern of CLV1 in the distal root meristem overlaps extensively with that of the transmembrane receptor kinase ACR4 [14], which regulates distal stem cell fate in a CLE40-dosage dependent manner [11] (Figures 1C, 1C′, and 1G). ACR4 was previously shown to undergo rapid turnover and internalization [20]. Upon dark incubation of ACR4-GFP reporter lines we now observed GFP signals in LysoTracker stainable vacuolar compartments similar to those noted for CLV1 (Figures 1D and 1F–1F″). This indicates that both CLV1 and ACR4 respond in a similar manner to CLE40. However, in contrast to *CLV1*, only *ACR4* is transcriptionally upregulated by CLE40 (Figures 1A–1D′ and Table S1). We used the transcriptional reporter pACR4:H2B-YFP and a translational fusion pACR4:ACR4-GFP and quantified the fluorescence intensities in the distal root meristem. With the transcriptional reporter, the *ACR4* expression domain expands within 6 hr after CLE40p treatment into the QC and the proximal meristem [11], and overall expression levels increase to almost 200% (Figures S1A–S1D and Table S1). The vacuolar ACR4-GFP signals of the translational fusion are found in all expressing cells, which indicates active signaling (Figure 1D′) [20]. The ACR4-GFP levels increase by only about 50% after CLE40p treatment (Table S1). This difference between the transcriptional and translational response can be explained by ligand induced rapid receptor turnover. Importantly, both CLV1 and ACR4 are expressed and signal in the same cells of the distal meristem, but only ACR4 is transcriptionally regulated by CLE40p (Table S1).

CLV1 and ACR4 Control Distal Root Meristem Maintenance

To assign a function to CLV1 signaling in the root, we analyzed *clv1* mutants (*clv1-20*, *clv1-21*, and *clv1-22*) [21] in the *Columbia* wild-type background (Figures 2 and S2 and Table S2). The distal part of the root consists of CCs containing starch granules for gravity perception (Figure 2A). CCs are

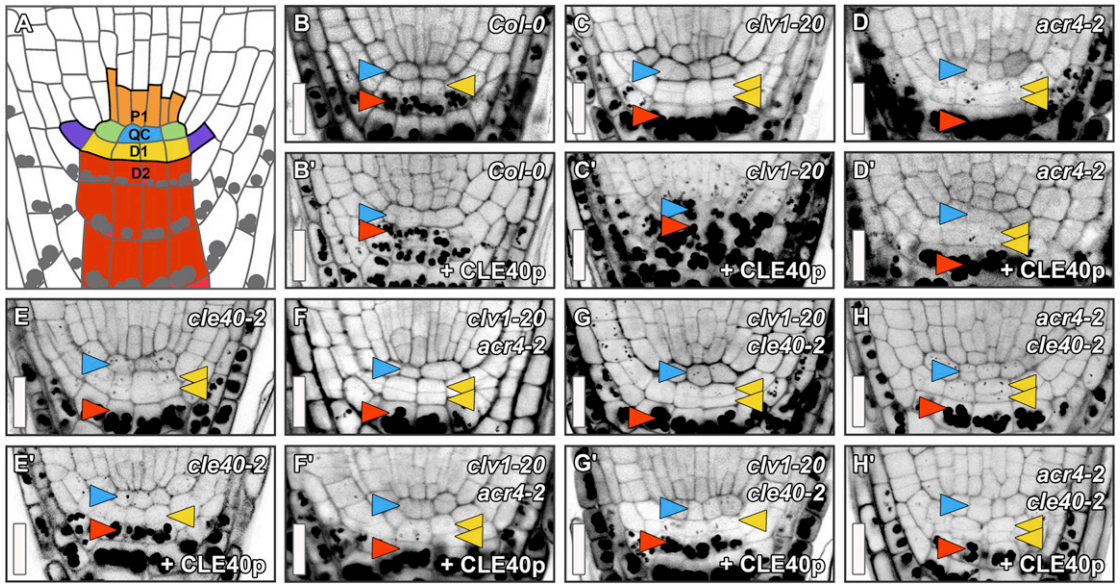

Figure 2. Functional Overlap of CLV1 and ACR4 in Distal Root Stem Cell Maintenance

(A) Diagram illustrating cell positions and cell fates in the *Arabidopsis* root meristem. Stem cells are outlined in black. Blue, QC; green, cortex endodermis initials; orange, proximal initials (P1); purple, lateral root cap/epidermis initials; yellow, CSCs (D1); red, CCs (D2); gray dots, starch granules.

(B–H′) Distal root cell fates were analyzed by mPSPI stainings of 5 days after germination wild-type (*Col-0*), *clv1-20*, *acr4-2*, and *cle40-2* single mutants (B–E′) and double-mutant combinations (F–H′). Root meristems grown on media with 200 nM CLE40 peptide (CLE40p) are shown (B′, C′, D′, E′, F′, G′, and H′). Arrowheads: blue, QC position; yellow, CSC position (D1); red, CC position (D2). Double yellow arrowheads indicate CSC fate in D2, whereas the lack of a yellow arrowhead indicates CC fate in D1 position.

Scale bars represent 20 μm. See also Figure S2 and Table S2 for data and statistics.

generated by CSCs that lack mPSPI stainable starch granules and form a single layer or, immediately after a cell division, two cell layers distal to the QC (Figures 2A, 2B, and S2 and Table S2). Similar to *cle40* and *acr4* mutants, *clv1* mutants also show additional CSC layers, indicating a role for CLV1 in CLE40-dependent distal stem cell regulation (Figures 2C–2E and S2 and Table S2). Increasing the dosage of CLE40 by growing *Arabidopsis* roots on medium containing synthetic CLE40p reduces stemness and causes differentiation of CSCs, QC cells, and P1 cells in the wild-type (Figures 2B′ and S2 and Table S2) [11]. CLE40p addition rescues *cle40* mutant roots and reduces stemness to almost wild-type levels, whereas *acr4* mutants show resistance to peptide treatment (Figures 2D′ and 2E′). This suggests that CLV1 only functions together with ACR4 or that CLV1 expression depends on ACR4. We therefore introduced the pCLV1:CLV1-GFP reporter into *acr4* and *cle40* mutant backgrounds and quantified fluorescence signal intensities. In the absence of ACR4, CLV1 was only expressed at 12% of wild-type levels, and CLV1 expression was reduced to 60% of wild-type levels in *cle40* mutant background (Table S1). This indicates that CLV1 expression is strongly dependent on ACR4 and to a lesser degree on CLE40 (Figure S1F). Surprisingly, *clv1* mutants show an even stronger loss of stemness upon CLE40p treatment than the wild-type (Figures 2C′ and S2 and Table S2). This indicates that CLV1 contributes to the CLE40-dependent stem cell restriction but is not necessary in the presence of excess CLE40p. Instead, CLV1 then serves to moderate stemness control pathways in the distal meristem.

Because ACR4 is transcriptionally upregulated by CLE40, whereas CLV1 is not, we suspected that ACR4 is responsible for this strong loss of stemness. In all double-mutant combinations of *cle40*, *clv1*, or *acr4*, increase of stemness was not additive, suggesting that these three genes act in a common pathway (Figures 2F–2H and S2 and Table S2). Nevertheless, double mutants of *clv1* with *acr4* displayed a slightly increased response to CLE40p compared to *acr4* single mutants, indicating that an additional stemness controlling pathway could be activated by ectopic CLE40p in the absence of CLV1 (Figures 2F′ and S2 and Table S2).

CLV1 and ACR4 Associate with Plasmodesmata

The observations that both CLV1 and ACR4 control stemness in the root meristem and their overlapping expression domains prompted us to test for their potential to interact at the molecular level employing FRET assays in *N. benthamiana*. To this end, translational fusions of both proteins to GFP or mCherry were generated and expressed from an inducible promoter to control protein expression levels. In *N. benthamiana* leaf epidermal cells, both ACR4 and CLV1 localized to the PM, which costained with the membrane dye FM4-64 (Figures 3A, 3A″, 3B, and 3B″). Interestingly, the ACR4-GFP fluorescence signal was more intense at immobile, cell-wall-localized punctate structures (Figure 3A, arrowheads). Because CRINKLY4, the ACR4 ortholog from maize, was previously found to localize to plasmodesmata (PDs) in the aleurone layer by immunogold transmission electron microscopy [22], we asked whether ACR4 or CLV1 also associate with PDs. PDs are plasma membrane-lined, regulated channels that permit the cell-to-cell transport of cytoplasmic molecules [23]. We used the fluorescent dye aniline blue, which labels callose, to visualize the callose-rich neck regions of PDs. We found a costaining of the punctate ACR4-GFP structures with aniline blue indicating that ACR4 preferentially associates with PDs, whereas CLV1 does not associate with PDs as strongly as ACR4 (Figures 3A–3A‴ and 3B–3B‴). ACR4-GFP still resided

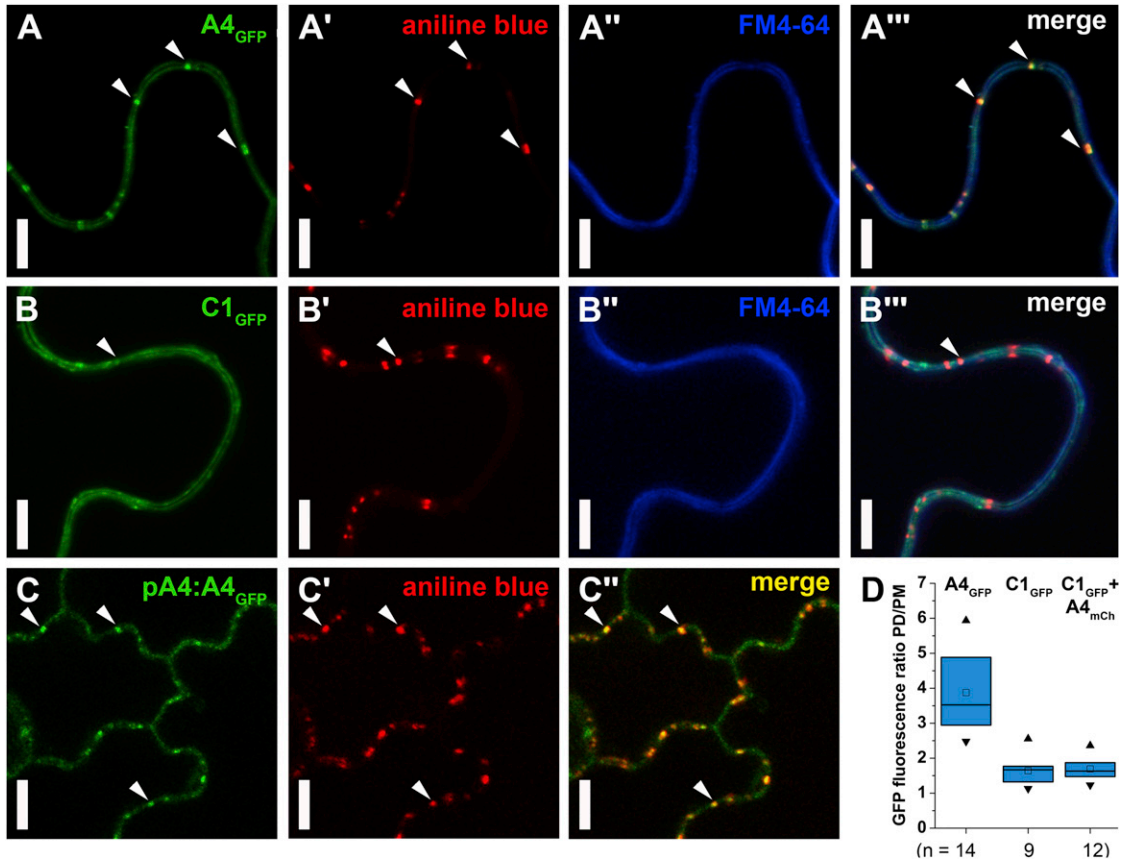

Figure 3. ACR4 and CLV1 Associate with Plasmodesmata

(A–C″) Subcellular localization of ACR4-GFP (A) and CLV1-GFP (B) in transiently expressing *N. benthamiana* leaf epidermal cells was analyzed with aniline blue for staining of callose/PDs (A′, B′, and C′) and FM4-64 for staining of the PM (A″ and B″). *pACR4:ACR4-GFP* in cotyledon epidermis of *Arabidopsis* was analyzed using aniline blue as callose/PD staining (C–C″). Arrowheads show examples of PD localizations. Scale bars represent 10 μm (A–B‴) or 5 μm (C–C″).

(D) GFP fluorescence ratios of PD/PM from transiently expressing *N. benthamiana* leaf epidermal cells are summarized in box plots. n, number of images analyzed; A4, ACR4; C1, CLV1.

See also Figure S3.

at the cell wall after retraction of the protoplast upon plasmolysis and costained with aniline blue (Figures S3C–S3C″). Here only one cell expresses ACR4-GFP, which explains why colocalization of aniline blue and ACR4-GFP at the cell wall overlaps only at the cell wall of the expressing cell and not the adjacent cells. CLV1-GFP showed a similar but weaker residual localization at cell walls after plasmolysis (Figures S3D–S3D″).

Further confirmation that the observed ACR4-GFP punctate structures at the cell wall are PDs came from colocalization experiments with known PD-associated proteins. We used GFP tagged versions of the viral MOVEMENT PROTEIN (MP) [24] and the PLASMODESMATA LOCALIZED PROTEIN1 (PDLP1) [25] and detected colocalization with ACR4-mCherry (Figures S3A–S3A″ and S3B–S3B″).

To quantify the differential accumulation we measured the intensity of the GFP fluorescence per pixel at the PM and PD regions. We found a 3.9-fold enrichment of ACR4 at PDs relative to the PM, comparable to the 6-fold PD enrichment observed for CRINKLY4 in maize aleurone cells [22] (Figure 3D). CLV1-GFP signals were 1.6-fold stronger at PDs than at the PM and coexpression of CLV1-GFP with ACR4-mCherry in *N. benthamiana* did not affect CLV1 localization (Figure 3D). We confirmed the association of ACR4 to PDs by costaining with aniline blue also in *Arabidopsis* cotyledons where ACR4 is expressed in the epidermal cell layer (Figures 3C–3C″) and by quantifying the fluorescence intensities at PDs and the PM. We found similar PD/PM ratios in *Arabidopsis* cotyledons as in *N. benthamiana* leaf cells (Figure S3G), and addition of CLE40p did not alter the localization of ACR4-GFP (Figures S3E–S3G).

CLV1 and ACR4 Can Interact In Planta

We found that CLV1 and ACR4 can interact in planta using a split luciferase assay (Figure S4). For a more-detailed study with subcellular resolution, we determined FRET between coexpressed GFP and mCherry receptor fusion proteins in transiently expressing *N. benthamiana* leaf epidermal cells (Figure 4). We chose the FRET pair GFP and mCherry as suitable fluorescent tracers for measurements close to the cell wall because the cell wall shows high autofluorescence in the emission spectrum of the more commonly used FRET pair CFP and YFP. FRET either between fluorophores with different spectra like GFP and mCherry (hetero-FRET) or between molecules with the same fluorescence spectrum only (homo-FRET) is strongly distance dependent on a nanometer length

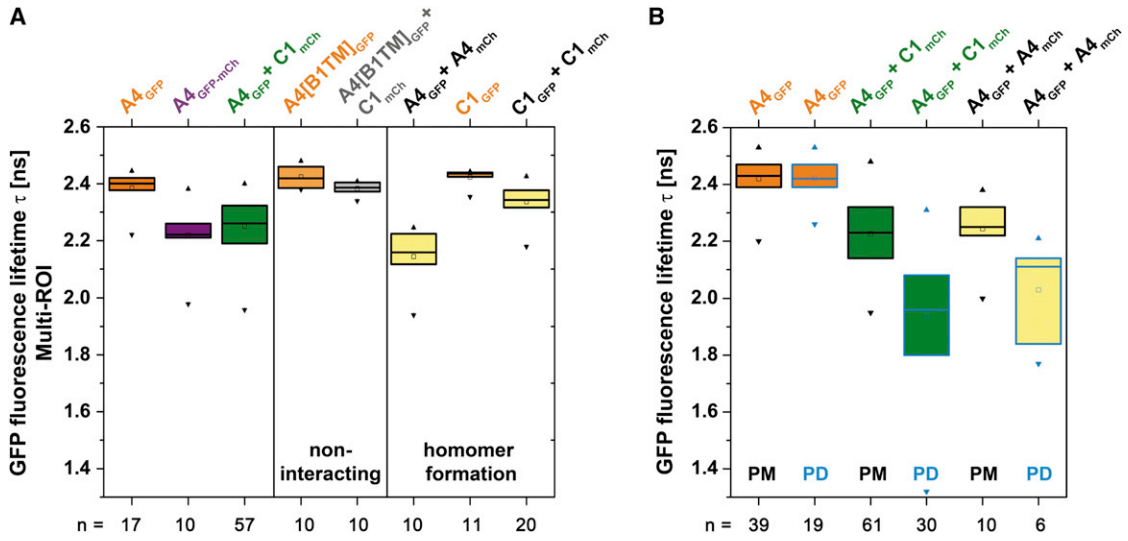

Figure 4. Interaction of CLV1 and ACR4 Measured by FRET-FLIM

GFP fluorescence lifetime τ (ns) was measured in transiently expressing *N. benthamiana* leaf epidermal cells. Fluorescence lifetime analyses of the indicated samples are summarized in box plots. A4, ACR4; C1, CLV1; B1, BAK1; mCh, mCherry.

(A) GFP fluorescence-weighted average lifetime fitted with a double-exponential model (Equation 5) with multi-ROI data of the indicated proteins at the plasma membrane.

(B) GFP fluorescence lifetime fitted pixel-wise with a monoexponential model (Equation 4) of the indicated proteins at the plasma membrane (PM) and at plasmodesmata (PD). Controls (GFP only) are depicted in orange, ACR4 and CLV1 heteromeric samples in green, and homomeric samples in yellow. The FRET-positive control (ACR4 fused to GFP-mCherry) is depicted in purple and the noninteracting heteromer of ACR4[BAK1TM]-GFP and CLV1-mCherry is depicted in gray.

Equations 4 and 5 can be found in the Supplemental Experimental Procedures. n, number of images analyzed. See also Figure S4 and Table S3 for data and statistics.

scale and therefore reports the interaction of the fused proteins [26].

In view of the wealth of distinct fluorescence methods with specific information, we used MFIS to collect the complete fluorescence information including FRET in a single measurement. We applied fluorescence lifetime analysis (FRET-FLIM) to use the donor fluorescence lifetime as intensity-independent parameter to measure protein interactions. The fluorescence of the donor (GFP) is quenched by the acceptor (mCherry) in case of hetero-FRET, and this leads to a reduction of the donor fluorescence lifetime, τ. In practice, expression and FRET systems are never homogeneous; often they contain a population of unquenched donor molecules. Thus, we analyzed the fluorescence lifetime of ACR4-GFP with a double-exponential fit model, which takes into account a population of unquenched donor molecules with a fluorescence lifetime τ = 2.39 ± 0.06 ns as well as a population undergoing FRET exhibiting a shorter fluorescence lifetime of 0.67 ± 0.12 ns. Here, the discovery of a population with shorter lifetime is a hallmark for FRET events (Figure S5D). For convenience, we used in the following the fluorescence-weighted average lifetime as indicator for FRET. Mean values refer to averaging over n samples.

The mean GFP fluorescence lifetime of ACR4-GFP alone at the PM is τ = 2.39 ± 0.06 ns (Figure 4A and Table S3). The positive control consisting of an ACR4-GFP-mCherry fusion showed a reduced mean fluorescence lifetime of τ = 2.22 ± 0.10 ns, indicating a significant intramolecular FRET. When ACR4-GFP and CLV1-mCherry were coexpressed, the lifetime was significantly reduced to τ = 2.25 ± 0.10 ns by intermolecular FRET, demonstrating that both receptors can interact (Figure 4A and Table S3). To investigate whether the interaction of CLV1 and ACR4 is specific and mediated by their transmembrane domains (TMDs), we exchanged the TMD of ACR4 against the TMD of BRI1 ASSOCIATED KINASE1 (BAK1), another PM-localized receptor kinase [27]. Coexpression of ACR4[BAK1TM]-GFP with CLV1-mCherry showed a lifetime of τ = 2.38 ± 0.02 ns, which is significantly different from ACR4-GFP and CLV1-mCherry (τ = 2.25 ± 0.10 ns) (Figure 4A and Table S3). This shows that interaction of ACR4 with CLV1 requires their specific TMDs. Previous assays with the TMDs of ACR4 in an *E. coli* system showed the capacity of TMDs to mediate homomeric interactions [28]. Here we found that ACR4 is able to form homomeric receptor complexes also in planta using FRET-FLIM analyses (ACR4-GFP + ACR4-mCherry: τ = 2.14 ± 0.10 ns) (Figure 4A and Table S3). Similarly, homomerization of CLV1 was shown with FRET acceptor photobleaching assays in planta [29], coimmunoprecipitation and split-luciferase assays [19, 30, 31], which we could verify by FRET-FLIM (CLV1-GFP: τ = 2.42 ± 0.03 ns; CLV1-GFP + CLV1-mCherry: τ = 2.34 ± 0.06 ns) (Figure 4A and Table S3).

Because we noted a strong association of ACR4 with PDs, we asked whether the interaction between CLV1 and ACR4 differs depending on their subcellular localization. Use of FRET-FLIM analyses with high spatial resolution enables to discriminate between different subcellular localizations, like the PM and PDs. We therefore compared FRET-FLIM analyses according to PM and PD localization. In order to conserve maximum spatial resolution, we fitted the fluorescence lifetime pixel-wise with a monoexponential model based on a maximum likelihood estimator, which is the statistically most efficient estimator for low photon numbers [32], but averages over all species populations and therefore yields also the

equivalent average fluorescence-weighted fluorescence lifetime (Figure 4B and Table S3). The mean fluorescence lifetime of the donor ACR4-GFP decreased in the presence of CLV1-mCherry from τ = 2.42 ± 0.07 ns to τ = 2.23 ± 0.12 ns at the PM, and to τ = 1.94 ± 0.21 ns at PDs. Similarly, ACR4 homomeric complexes show a reduction of the ACR4-GFPs mean fluorescence lifetime at PDs (τ = 2.03 ± 0.18 ns) compared to the PM (τ = 2.24 ± 0.12 ns) (Figure 4B and Table S3). We were not yet able to separate CLV1 homomeric complexes formed at PDs from those at the PM. Together these FRET-FLIM analyses demonstrate that ACR4 and CLV1 form homomeric and heteromeric complexes with distinct stoichiometries or conformations depending on their different subcellular localizations.

CLV1 and ACR4 Form Localization-Dependent Homo- and Heteromeric Complexes

In order to differentiate heteromeric and homomeric complexes and their composition, we used MFIS, which allows for a novel two-dimensional FRET analysis. Here, in addition to the fluorescence lifetime τ as a measure for hetero-FRET, which allows detecting the formation of heteromeric complexes, we also determined the steady-state fluorescence anisotropy *r* which describes fluorescence depolarization.

Fluorescence anisotropy increases due to hindered rotational mobility of a protein, e.g., by its incorporation into a protein complex. However, a decrease of fluorescence anisotropy is observed when homo-FRET occurs, the energy transfer between GFP molecules only [26, 33] (Figure S5A).

When a freely diffusing GFP was expressed in *N. benthamiana*, we found a mean fluorescence anisotropy of *r* = 0.332 ± 0.005 (n = 10), in agreement with published values [26] (Table S4). For the fusion of GFP to ACR4, we would expect a reduced rotational freedom and therefore an increase in anisotropy compared to free GFP. However, we found an anisotropy even lower than that for free GFP (ACR4-GFP: *r* = 0.300 ± 0.013, n = 11, Table S4), which can be attributed to homo-FRET between ACR4-GFP in homomeric complexes. To test for this assumption, we performed progressive photobleaching of ACR4-GFP, which serves to reduce the occurrence of homo-FRET events. Now anisotropy increased to the levels of free GFP, indicating that ACR4 tends to form homomers (Figures S5A–S5C).

To examine the formation of homo- and heteromeric complexes simultaneously and with maximal spatial resolution, we generated the fluorescence intensity, lifetime, and anisotropy images for MFIS analyses. Two exemplary MFIS data sets of donor only sample ACR4-GFP and the FRET sample ACR4-GFP + CLV1-mCherry are shown in Figures 5A–5B″. Using the intensity information in ACR4-GFP-expressing cells, we can distinguish PM and PD regions and analyze their local fluorescence lifetime and anisotropy pixel-wise. We noted that anisotropy was lower at PDs compared to the PM (Table S4), while fluorescence lifetime was unaffected. To distinguish the spatially dependent composition of different complexes, we analyzed two-dimensional pixel frequency histograms of fluorescence anisotropy *r* versus fluorescence lifetime τ, with the corresponding one-dimensional distributions given as projection (Figure 5C). Considering ACR4-GFP (Figures 5A–5A″), pixels originating from PDs form a subpopulation (red pixel population, Figure 5C) with a distinctly lower anisotropy than those from the PM (orange pixel population, Figure 5C). Both fluorescence lifetime and fluorescence depolarization affect fluorescence steady-state anisotropy, which is described by the Perrin equation (see the Experimental Procedures). The Perrin line for freely diffusing GFP served as a reference to identify homo-FRET (below the black line, Figure 5C) and hindered rotational mobility (above the black line, Figure 5C). Both PM (orange) and PD (red) populations of ACR4-GFP center below the Perrin line, which indicates homo-FRET and therefore homomer formation of ACR4. Homo-FRET is much stronger at PDs than at the PM (Table S4). When ACR4-GFP was coexpressed with CLV1-mCherry (Figures 5B–5B″), a decrease of fluorescence lifetime τ indicated hetero-FRET and heteromerization of the two receptors at the PM (green pixel population, Figure 5C). Additionally, anisotropy above the Perrin line was observed, probably due to hindered mobility of GFP in the formed complex. Again, complex composition differed at PDs (blue pixel population, Figure 5C). Here, both τ and *r* strongly decreased, indicating a preferential formation of more, or higher-order, homomeric complexes consisting of ACR4, and additionally of heteromeric complexes of ACR4 and CLV1 at these sites (Figure 5C). Thus, we hypothesize that the composition of complexes strongly depends on local concentration differences of the two receptors, and their local environments (Figure 5D).

Discussion

We show here that CLV1, a receptor kinase regulating shoot stemness, is expressed in root meristems and has an additional function in root stemness control. Like in the shoot, CLV1 signaling leads to a removal of CLV1 from the PM and ultimately degradation in lytic vacuoles. *clv1* mutants show supernumerary CSCs, and accumulation of CLV1 in lytic vacuoles is more pronounced in that domain. *CLV1* is also expressed in epidermis and lateral root cap cells, where we did not notice any mutant phenotype so far. Both mutant phenotype and expression pattern overlap with that of ACR4. Double-mutant analyses indicate that CLV1 and ACR4 act in the same pathway to regulate distal stem cell number in *Arabidopsis*. Interestingly, only *ACR4*, but not *CLV1* is transcriptionally upregulated upon ectopic CLE40p treatments and shows increased signaling and differentiation.

From these observations, we propose a model explaining distal stemness regulation in the *Arabidopsis* root meristem, based on the functions of two different receptor complexes and their concentrations. Cells at the D1 and D2 position coexpress CLV1 and ACR4, and in these cells, different types of complexes can be formed. Our FRET-FLIM data demonstrated that both receptors are capable of forming homomeric and heteromeric complexes. Extending these analyses by employing MFIS allowed us to distinguish complex types at subcellular resolution. Both proteins localize to the PM, where they can form homo- and heteromeric complexes. However, at PDs, the local concentration of ACR4 is increased, whereas CLV1 does not accumulate there to the same extend. This locally high concentration fosters the formation of ACR4 homomeric complexes in addition to heteromeric complexes with CLV1.

We propose that during normal development, both types of complexes are required to repress stemness in the D2 cell layer and promote columella cell differentiation. In *clv1* mutants, only ACR4 homomeric complexes can be formed, and these fail to repress stemness in the distal root meristem. However, ectopic CLE40p stimulation induces increased ACR4 expression also in cells that normally lack CLV1, such as the QC and P1 cells. Here, ACR4 homomeric complexes

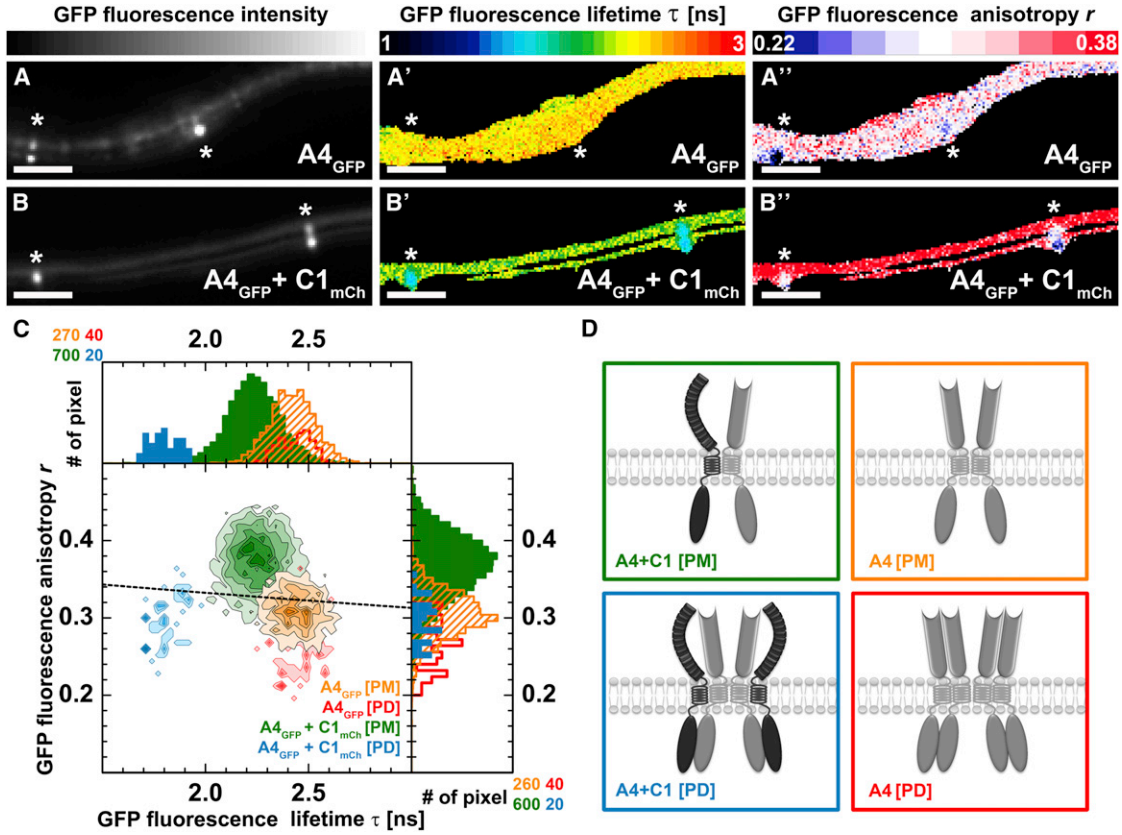

Figure 5. MFIS Reveals Localization of Specific Homomer and Heteromer Formation of CLV1 and ACR4

(A–B″) Fluorescence intensity images of ACR4-GFP (A), and ACR4-GFP + CLV1-mCherry (B) of transiently expressing *N. benthamiana* leaf epidermal cells. (A′) and (B′) show fluorescence lifetime images of the cells in (A) and (B). Fluorescence anisotropy images of these cells are shown in (A″) and (B″). GFP fluorescence lifetime τ [ns] and GFP fluorescence anisotropy *r* are color coded. Pixels with a photon number too low for sufficient fitting are displayed in black. Scale bars represent 2 μm. Asterisks mark the localization of PDs.

(C) 2D frequency histograms of MFIS data derived from the images in (A′) and (A″) (ACR4-GFP) and (B′) and (B″) (ACR4-GFP + CLV1-mCh). GFP fluorescence lifetime τ (ns) is plotted on the x axis, and GFP fluorescence anisotropy *r* is plotted on the y axis. The black line represents the Perrin equation corresponding to freely diffusing GFP in aqueous buffer.

(D) Model of homomer formation of ACR4 (gray receptors) and heteromer formation with CLV1 (black receptors) at the PM or PDs corresponding to the color coded populations in (C). A4, ACR4; C1, CLV1; [PM], plasma membrane; [PD], plasmodesmata.

See also Figure S5 and Table S4.

can now promote ectopic acquisition of columella cell identity and differentiation. In *acr4* mutants, CLV1 alone is insufficient for distal stemness regulation. The observation that *clv1* mutants display increased stem cell numbers but also respond even more strongly to CLE40p suggests that CLV1 moderates ACR4-dependent signaling by binding to ACR4, thereby creating also heteromeric complexes.

In both shoot and root meristems, non-cell-autonomous signaling between OC or QC and stem cells controls their maintenance. The localization of both ACR4 and CLV1 at the PM and PDs is intriguing. CLV1 has previously been implicated only in transcriptional regulation of the stem cell regulator WUS in shoot meristem development. How CLV1 can actually transmit a signal to the nucleus is not known in detail, but CLV1 kinase activity and POLTERGEIST-LIKE phosphatases are required for this process [34]. Our finding that CLV1 and ACR4 can interact at PDs could implicate an ACR4/CLV1 receptor complex controlling stemness in a more direct manner. Maintenance of CSCs is regulated by signals emanating from the QC. These two cell types are connected by on average three PDs per μm^2 [35]. PD-localized ACR4/CLV1 complexes could directly regulate or restrict the mobility of these signals (e.g., stemness factors) and thereby confine stem cell identity to a single cell layer in direct contact with the QC. Conceptually similar, regulated transport through PDs has been proposed for the SHORTROOT (SHR) [36] protein, which acts from the stele to control identity in the adjacent cell layer. Alternatively, increased accumulation of ACR4 at PDs may serve to locally increase receptor concentration and foster ACR4 homomerization. Thus, PDs could serve as signaling centers in plants, similar to the role of cilia in hedgehog signaling of animal cells [37].

Apart from its role in regulating the root meristem development, ACR4 has a more general role in maintaining cell layer integrity and the control of formative cell divisions throughout development [13, 14, 22, 38, 39]. In maize, the ACR4 ortholog CR4 associates with PDs that connect aleurone cells. Here, CR4 was proposed to enhance the lateral mobility of an aleurone signaling molecule [22]. In the *Arabidopsis* shoot system, ACR4 is expressed in epidermal cell layers starting from the outermost (L1) layer of the shoot meristem. However, stemness regulation in shoot meristems is mediated by CLV1 and CLV2/CRN, but does not depend on ACR4 function.

Our discovery that CLV1 functions in root stemness control extends the homologies between the shoot and root stem cell niches. The ancestral shoot stem cell regulator may have consisted of CLV3, CLV1, and WUS orthologs. Both ACR4 and CLV1 orthologs are already present in bryophytes that lack a typical root meristem [17]. The evolution of a root stem cell niche with a distinct, layered organization compared to the shoot system thus may have necessitated the recruitment of ACR4 into a stemness signaling pathway by CLV1.

Experimental Procedures

Mutants and Reporter Lines

T-DNA insertion lines *clv1-20* (SALK008670) and *clv1-21* (SAIL802_C08) in the *Col-0* and *clv1-22* (WiscDsLox489-492B1) in the *Col-2* background were described [21] and were obtained from the Nottingham *Arabidopsis* Stock Center (NASC, UK). The sites of the T-DNA insertions and their distal root phenotypes are depicted in Figure S2. The pACR4:ACR4-GFP reporter line was described previously and provided by Gwyneth Ingram [20]. The pCLV1:CLV1-GFP reporter line was constructed by PCR amplification of 3,087 bp upstream of the start codon plus the whole CLV1 coding region without stop codon (2,938 bp) and recombination into a modified pMDC99 [40] with C-terminal eGFP in frame after the attR2 site. The pCLV1:CLV1-GFP reporter was introduced into the *clv1-11* mutant and complemented the *clv1* shoot phenotypes in 17 of 30 plants. Construction of estradiol inducible expression vectors with GFP, mCherry, and GFP-mCherry as translational fusions at the C terminus for transient expression in *N. benthamiana* leaves was described previously [29]. The following expression clones have been generated to produce inducible translational fusions with fluorescent proteins: CLV1 (aa 1–979) and ACR4 (aa 1–895), all without a stop codon in frame with eGFP and/or mCherry. For ACR4[BAK1TM], the ACR4 TM (IATAEIGFALFLVAVVSITAALYI) was exchanged with the BAK1 TM (ITGAIAGGVAAGAALLFAVPAIALAWW) via the "gene fusion" protocol described earlier [41]. For the split *Renilla* luciferase complementation experiments, the following estradiol inducible expression clones have been generated: CLV1Δkinase (aa 1–689), ACR4Δkinase (aa 1–497), and BAK1 (aa 1–615), all without a stop codon in frame with the N- or C-terminal part of the Renilla luciferase as described [42].

Plant Growth Conditions and Peptide Treatments

Arabidopsis plants were grown on growth medium (GM) plates as described [11]. For peptide treatments, GM plates supplemented with 200 nM CLE40p (RQV<u>P</u>TGSDPLHHK; the underlined P is hydroxyproline) were used. *Nicotiana benthamiana* plants were grown for 4 weeks in a greenhouse under controlled conditions. Transient expression of proteins in *N. benthamiana* was carried out as described previously [29]. Transgene expression was induced 48 to 96 hr after infiltration with 20 μM β-estradiol and 0.1% Tween 20 and analyzed 12–24 hr after induction.

Stainings

mPSPI staining and root imaging was done as described previously [43]. Callose stainings were done by infiltration of a 0.1 mg/ml solution of aniline blue (Biosupplies) into *N. benthamiana* leaves or incubation of *Arabidopsis* cotyledons for 1 hr. Counterstaining of the root cell wall was achieved with 10 μM propidium iodide (PI). Plasma membrane staining was carried out with 20 μM FM4-64. LysoTracker Red (Invitrogen) was used to stain lytic vacuoles by incubating roots for 5 min in a 2 μM solution.

Plasmolysis

Transiently expressing *N. benthamiana* leaves were infiltrated with 30% glycerol and imaged immediately.

Microscopy

For imaging either a confocal laser scanning microscope Zeiss LSM780 or Olympus FV1000 was used. GFP was excited at 488 nm and emission detected at 490–560 nm. PI and FM4-64 were excited at 561 or 559 nm and emission detected with a long-pass 590 nm or at 575–620 nm, respectively. LysoTracker Red was excited with 561 nm and detected at 575–620 nm. Aniline blue was excited at 405 nm and emission detected at 415–480 nm. Image acquisition was always carried out sequentially to prevent crosstalk between channels.

Fluorescence Signal Intensity

Fluorescence signal intensity was analyzed with ImageJ software (http://rsb.info.nih.gov/ij/) and data were statistically evaluated with Microsoft Excel 2010. Fluorescence signal intensities (mean gray values) of reporter lines pACR4:ACR4-GFP and pCLV1:CLV1-GFP were obtained in a 400 × 100 pixel region of interest (ROI) (at 0.11 μm/pixel) just below the QC covering D1 and D2 positions and background subtracted with mean gray values from wild-type roots imaged with the same settings.

PD/PM Fluorescence Intensity Ratio

PD/PM fluorescence intensity ratio was determined by measurement of the intensity values of the GFP channel in three PM and three PD regions (10 × 10 pixel, 0.11 μm/pixel) in each image with ImageJ. The obtained values for fluorescence intensities are displayed in box plots created with OriginPro 8.0 (OriginLab). Boxes represent the 25th to 75th percentile. The square represents the mean value and the line represents the median. Black triangles represent the minimum and maximum values (outliers).

Split *Renilla* Luciferase Complementation Assay

After overnight induction with 20 μM β-estradiol and 0.1% Tween 20, one-half of transiently expressing *N. benthamiana* leaves were infiltrated with 10 μM ViviRen (Invitrogen) substrate and assayed as described [42].

Multiparameter Fluorescence Image Spectroscopy

MFIS was performed with a multiparameter fluorescence detection setup with the corresponding fluorescence lifetime and anisotropy analyses as described previously [32, 44]. Experiments were performed with a confocal laser scanning microscope (Olympus FV1000, IX81 inverted microscope) additionally equipped with a single-photon counting device with picosecond time resolution (PicoQuant Hydra Harp 400). GFP was excited at 485 nm with a linearly polarized, pulsed (40 MHz) diode laser (LDH-D-C-485) at 1.2 μW at the objective (60× water immersion, Olympus UPlanSApo NA 1.2, diffraction limited focus). The emitted light was collected in the same objective and separated into its perpendicular and parallel polarization (Thorlabs PBS 101). Fluorescence was then detected by SPADs (MPD, PD5CTC) in a narrow range of GFP's emission spectrum (band-pass filter: HC520/35 AHF). Images were taken with 100 μs pixel time and a resolution of 96 nm/pixel. A series of 20 frames were merged into one image and further analyzed [45].

Single-Pixel Fluorescence Lifetime Analyses

The fluorescence lifetime of GFP was determined pixel-wise in merged images to increase photon numbers for analysis. The histograms presenting the decay of fluorescence intensity after the excitation pulse contained typically 500–4,000 photons and were built for each pixel with 128 ps per bin.

In fluorescence lifetime, microscopy with high spatial resolution and low excitation power to prevent photobleaching the number of photons per pixel is exceptionally low. Therefore, a model to fit the data with a minimal number of parameters has to be applied in conjunction with a maximum likelihood estimator (MLE) [32]. We are aware that GFP alone has already a biexponential fluorescence decay [46], which becomes even more complex in the presence of additional FRET species. This generally multiexponential decay is approximated in the subsequent fluorescence lifetime analysis by an (fluorescence-weighted) average lifetime, τ. We therefore used a monoexponential model function with two variables (fluorescence lifetime τ and scatter contribution γ; for details, see the Supplemental Experimental Procedures) fitted with MLE. The instrument response function was measured with the backreflection of the laser beam and used for iterative reconvolution in the fitting process (see the Supplemental Experimental Procedures, Equation 4). This approach delivers the average fluorescence lifetime as a stable parameter even in critical surroundings with high background and low expression levels.

Multi-ROI Fluorescence Lifetime Analyses

Heterogeneity of the expression system leads to a population of donor molecules undergoing FRET and a population of unquenched donor molecules. This population probably originates from unmatured acceptor molecules as it has been reported earlier for fluorescent proteins of the DsRed family [45]. A common description of such a situation is a double-exponential model with one lifetime for the unquenched donor population and FRET population, respectively. The lifetime of the unquenched donor is determined from GFP in the absence of mCherry using a monoexponential fit and is kept constant in the following double-exponential analyses (see the Supplemental Experimental Procedures, Equation 5). The second lifetime

corresponds to the GFP population undergoing FRET. The fluorescence-weighted average lifetime is displayed. We selected typically 400–700 pixels per merged image ("multi-ROI") of the PM region and used all photons to build the histogram of the fluorescence decay with 128 ps per bin.

Anisotropy Analyses

The steady-state anisotropy is given by $r = \frac{GF_{\parallel} - F_{\perp}}{(1 - 3l_1)GF_{\parallel} + (2 - 3l_2) \cdot F_{\perp}}$. The fluorescence signal of GFP with parallel and perpendicular polarizations is denoted as $F_{\parallel}$ and $F_{\perp}$, respectively. The ratio G of the detection efficiencies g of the perpendicular and parallel polarized light is given as $G = g_{\perp}/g_{\parallel}$. The G factor of the setup was determined by calibration measurements with the dye Rhodamine 110. The factors l_1 and l_2 above account for polarization mixing due to the objective lens as described in [47]. These factors can be determined for a given microscope in a separate calibration measurement [48]. The fluorescence signal was also corrected for dead time of the detection electronics following $s_{det} = \frac{s_{rec}}{1 - s_{rec} * t_d}$ [49], with s_{det} for the detected signal, s_{rec} for the recorded signal and t_d for the dead time of the detector, respectively.

FRET-FLIM Data Presentation

(1) In each FRET-FLIM image, single-pixel fluorescence lifetimes were averaged across a representative region of interest (ROI), containing the PM or PDs of two neighboring cells, respectively. (2) In each FRET-FLIM image, a multi-ROI containing the PM was selected and analyzed according to the procedure described above. The obtained values from (1) and (2) for fluorescence lifetime are displayed in box plots created with OriginPro 8.6 (OriginLab). Boxes represent the 25th to 75th percentile. The square represents the mean value and the line represents the median. Black triangles represent the minimum and maximum values (outliers). n represents the number of taken FRET-FLIM images and, therefore, the number of measured cell pairs.

Lifetime and Anisotropy Images

The resulting images show the corresponding fluorescence lifetime τ for each pixel in a rainbow color code from navy (τ = 1 ns) to red (τ = 3 ns) and anisotropy r in a three color code from navy (r = 0.22) to red (r = 0.38). Pixels with a photon number too low for sufficient fitting are displayed in black.

2D Plot

Fluorescence anisotropy and lifetime were plotted in two-dimensional frequency histograms, where the number of pixels is displayed. The binning is as follows: lifetime 30 ps, anisotropy 0.008, seven levels, respectively.

Perrin Equation

The Perrin equation describes fluorescence depolarization due to rotational diffusion and, therefore, correlates measured fluorescence anisotropy r, rotational correlation time ρ, and fluorescence lifetime τ: $r = \frac{r_0}{(1 + \tau/\rho)}$, where r_0 denotes the fundamental anisotropy. The Perrin equation for freely diffusing GFP in aqueous buffer served as reference for other GFP fusion proteins and complexes, using r_0 = 0.38 and ρ = 14 ns as described in [26].

This reference represents the lower limit for the anisotropy of a GFP chromophore affected by rotational motion only. Influences like the viscosity in the cytoplasm or hindered rotation due to the fusion to a protein or complex formation can only increase the anisotropy value and therefore not explain low anisotropies. Possible preferential orientation due to the membrane environment has not been observed in the presented system.

Progressive Photobleaching

We performed photobleaching experiments on ACR4-GFP transiently expressed in epidermal leaf cells in *N. benthamiana* using a microscopy setup as described. GFP was continuously photobleached by taking image series of 40 frames at 1.5 μW at the objective with a long pixeltime of 400 μs and high spatial resolution (96 nm/pixel). For each image series fluorescence intensity and anisotropy were determined over time in regions of interest containing typically 50 pixels.

Accession Numbers

Sequence data from this article can be found in the Arabidopsis Genome Initiative or GenBank/EMBL databases under the following accession numbers: At3G59420 (ACR4), At1G75820 (CLV1), At5G12990 (CLE40), and At4G33430 (BAK1).

Supplemental Information

Supplemental Information includes Supplemental Experimental Procedures, five figures, and four tables and can be found with this article online at http://dx.doi.org/10.1016/j.cub.2013.01.045.

Acknowledgments

We thank Silke Winters, Carin Theres, and Cornelia Gieseler for technical assistance in the lab, Stanislav Kalinin for fluorescence analyses programs, the NASC for seeds, and Marcel Lafos, Daniel Schubert, and Thomas Klein for critical discussion of the manuscript. We thank Eduardo de la Peña for providing the PDLP1-GFP and MP-GFP constructs. We would like to acknowledge the Center of Advanced Imaging (CAI) at the Heinrich Heine University Düsseldorf. This work was supported by a grant of the Deutsche Forschungsgemeinschaft (DFG) to R.S. and C.A.M.S through SFB590.

Received: May 31, 2012
Revised: December 21, 2012
Accepted: January 15, 2013
Published: February 7, 2013

References

1. Scheres, B. (2007). Stem-cell niches: nursery rhymes across kingdoms. Nat. Rev. Mol. Cell Biol. *8*, 345–354.
2. Schoof, H., Lenhard, M., Haecker, A., Mayer, K.F., Jürgens, G., and Laux, T. (2000). The stem cell population of Arabidopsis shoot meristems in maintained by a regulatory loop between the CLAVATA and WUSCHEL genes. Cell *100*, 635–644.
3. Yadav, R.K., Perales, M., Gruel, J., Girke, T., Jönsson, H., and Reddy, G.V. (2011). WUSCHEL protein movement mediates stem cell homeostasis in the Arabidopsis shoot apex. Genes Dev. *25*, 2025–2030.
4. Nimchuk, Z.L., Tarr, P.T., Ohno, C., Qu, X., and Meyerowitz, E.M. (2011). Plant stem cell signaling involves ligand-dependent trafficking of the CLAVATA1 receptor kinase. Curr. Biol. *21*, 345–352.
5. Clark, S.E., Williams, R.W., and Meyerowitz, E.M. (1997). The CLAVATA1 gene encodes a putative receptor kinase that controls shoot and floral meristem size in Arabidopsis. Cell *89*, 575–585.
6. Ogawa, M., Shinohara, H., Sakagami, Y., and Matsubayashi, Y. (2008). Arabidopsis CLV3 peptide directly binds CLV1 ectodomain. Science *319*, 294.
7. Brand, U., Fletcher, J.C., Hobe, M., Meyerowitz, E.M., and Simon, R. (2000). Dependence of stem cell fate in Arabidopsis on a feedback loop regulated by CLV3 activity. Science *289*, 617–619.
8. Müller, R., Bleckmann, A., and Simon, R. (2008). The receptor kinase CORYNE of Arabidopsis transmits the stem cell-limiting signal CLAVATA3 independently of CLAVATA1. Plant Cell *20*, 934–946.
9. Sarkar, A.K., Luijten, M., Miyashima, S., Lenhard, M., Hashimoto, T., Nakajima, K., Scheres, B., Heidstra, R., and Laux, T. (2007). Conserved factors regulate signalling in Arabidopsis thaliana shoot and root stem cell organizers. Nature *446*, 811–814.
10. Doerner, P. (1998). Root development: quiescent center not so mute after all. Curr. Biol. *8*, R42–R44.
11. Stahl, Y., Wink, R.H., Ingram, G.C., and Simon, R. (2009). A signaling module controlling the stem cell niche in Arabidopsis root meristems. Curr. Biol. *19*, 909–914.
12. Hobe, M., Müller, R., Grünewald, M., Brand, U., and Simon, R. (2003). Loss of CLE40, a protein functionally equivalent to the stem cell restricting signal CLV3, enhances root waving in Arabidopsis. Dev. Genes Evol. *213*, 371–381.
13. Gifford, M.L., Dean, S., and Ingram, G.C. (2003). The Arabidopsis ACR4 gene plays a role in cell layer organisation during ovule integument and sepal margin development. Development *130*, 4249–4258.
14. De Smet, I., Vassileva, V., De Rybel, B., Levesque, M.P., Grunewald, W., Van Damme, D., Van Noorden, G., Naudts, M., Van Isterdael, G., De Clercq, R., et al. (2008). Receptor-like kinase ACR4 restricts formative cell divisions in the Arabidopsis root. Science *322*, 594–597.
15. Fiers, M., Golemiec, E., Xu, J., van der Geest, L., Heidstra, R., Stiekema, W., and Liu, C.M. (2005). The 14-amino acid CLV3, CLE19, and CLE40

peptides trigger consumption of the root meristem in Arabidopsis through a CLAVATA2-dependent pathway. Plant Cell *17*, 2542–2553.

16. Replogle, A., Wang, J., Bleckmann, A., Hussey, R.S., Baum, T.J., Sawa, S., Davis, E.L., Wang, X., Simon, R., and Mitchum, M.G. (2011). Nematode CLE signaling in Arabidopsis requires CLAVATA2 and CORYNE. Plant J. *65*, 430–440.
17. Miwa, H., Tamaki, T., Fukuda, H., and Sawa, S. (2009). Evolution of CLE signaling: origins of the CLV1 and SOL2/CRN receptor diversity. Plant Signal. Behav. *4*, 477–481.
18. Tamura, K., Shimada, T., Ono, E., Tanaka, Y., Nagatani, A., Higashi, S.I., Watanabe, M., Nishimura, M., and Hara-Nishimura, I. (2003). Why green fluorescent fusion proteins have not been observed in the vacuoles of higher plants. Plant J. *35*, 545–555.
19. Guo, Y., Han, L., Hymes, M., Denver, R., and Clark, S.E. (2010). CLAVATA2 forms a distinct CLE-binding receptor complex regulating Arabidopsis stem cell specification. Plant J. *63*, 889–900.
20. Gifford, M.L., Robertson, F.C., Soares, D.C., and Ingram, G.C. (2005). ARABIDOPSIS CRINKLY4 function, internalization, and turnover are dependent on the extracellular crinkly repeat domain. Plant Cell *17*, 1154–1166.
21. Durbak, A.R., and Tax, F.E. (2011). CLAVATA signaling pathway receptors of Arabidopsis regulate cell proliferation in fruit organ formation as well as in meristems. Genetics *189*, 177–194.
22. Tian, Q., Olsen, L., Sun, B., Lid, S.E., Brown, R.C., Lemmon, B.E., Fosnes, K., Gruis, D.F., Opsahl-Sorteberg, H.G., Otegui, M.S., and Olsen, O.A. (2007). Subcellular localization and functional domain studies of DEFECTIVE KERNEL1 in maize and Arabidopsis suggest a model for aleurone cell fate specification involving CRINKLY4 and SUPERNUMERARY ALEURONE LAYER1. Plant Cell *19*, 3127–3145.
23. Maule, A.J., Benitez-Alfonso, Y., and Faulkner, C. (2011). Plasmodesmata - membrane tunnels with attitude. Curr. Opin. Plant Biol. *14*, 683–690.
24. Lee, J.Y., Taoka, K.-I., Yoo, B.-C., Ben-Nissan, G., Kim, D.-J., and Lucas, W.J. (2005). Plasmodesmal-associated protein kinase in tobacco and Arabidopsis recognizes a subset of non-cell-autonomous proteins. Plant Cell *17*, 2817–2831.
25. Thomas, C.L., Bayer, E.M., Ritzenthaler, C., Fernandez-Calvino, L., and Maule, A.J. (2008). Specific targeting of a plasmodesmal protein affecting cell-to-cell communication. PLoS Biol. *6*, e7.
26. Borst, J.W., and Visser, A.J.W.G. (2010). Fluorescence lifetime imaging microscopy in life sciences. Meas. Sci. Technol. *21*, 102002.
27. Postel, S., Küfner, I., Beuter, C., Mazzotta, S., Schwedt, A., Borlotti, A., Halter, T., Kemmerling, B., and Nürnberger, T. (2010). The multifunctional leucine-rich repeat receptor kinase BAK1 is implicated in Arabidopsis development and immunity. Eur. J. Cell Biol. *89*, 169–174.
28. Stokes, K.D., and Gururaj Rao, A. (2008). Dimerization properties of the transmembrane domains of Arabidopsis CRINKLY4 receptor-like kinase and homologs. Arch. Biochem. Biophys. *477*, 219–226.
29. Bleckmann, A., Weidtkamp-Peters, S., Seidel, C.A.M., and Simon, R. (2010). Stem cell signaling in Arabidopsis requires CRN to localize CLV2 to the plasma membrane. Plant Physiol. *152*, 166–176.
30. Kinoshita, A., Betsuyaku, S., Osakabe, Y., Mizuno, S., Nagawa, S., Stahl, Y., Simon, R., Yamaguchi-Shinozaki, K., Fukuda, H., and Sawa, S. (2010). RPK2 is an essential receptor-like kinase that transmits the CLV3 signal in Arabidopsis. Development *137*, 3911–3920.
31. Zhu, Y., Wang, Y., Li, R., Song, X., Wang, Q., Huang, S., Jin, J.B., Liu, C.-M., and Lin, J. (2010). Analysis of interactions among the CLAVATA3 receptors reveals a direct interaction between CLAVATA2 and CORYNE in Arabidopsis. Plant J. *61*, 223–233.
32. Weidtkamp-Peters, S., Felekyan, S., Bleckmann, A., Simon, R., Becker, W., Kühnemuth, R., and Seidel, C.A.M. (2009). Multiparameter fluorescence image spectroscopy to study molecular interactions. Photochem. Photobiol. Sci. *8*, 470–480.
33. Bader, A.N., Hoetzl, S., Hofman, E.G., Voortman, J., van Bergen en Henegouwen, P.M., van Meer, G., and Gerritsen, H.C. (2011). Homo-FRET imaging as a tool to quantify protein and lipid clustering. ChemPhysChem *12*, 475–483.
34. Song, S.-K.K., Lee, M.M., and Clark, S.E. (2006). POL and PLL1 phosphatases are CLAVATA1 signaling intermediates required for Arabidopsis shoot and floral stem cells. Development *133*, 4691–4698.
35. Zhu, T., Quinn, R.L.O., Lucas, W.J., and Rost, T.L. (1998). Directional cell-to-cell communication in the Arabidopsis root apical meristem II. Dynamics of plasmodesmatal formation. Protoplasma *204*, 84–93.
36. Vatén, A., Dettmer, J., Wu, S., Stierhof, Y.D., Miyashima, S., Yadav, S.R., Roberts, C.J., Campilho, A., Bulone, V., Lichtenberger, R., et al. (2011). Callose biosynthesis regulates symplastic trafficking during root development. Dev. Cell *21*, 1144–1155.
37. Goetz, S.C., and Anderson, K.V. (2011). The primary cilium: a signaling center during vertebrate development. Nat. Rev. Genet. *11*, 331–344.
38. Watanabe, M., Tanaka, H., Watanabe, D., Machida, C., and Machida, Y. (2004). The ACR4 receptor-like kinase is required for surface formation of epidermis-related tissues in Arabidopsis thaliana. Plant J. *39*, 298–308.
39. Tanaka, H., Watanabe, M., Watanabe, D., Tanaka, T., Machida, C., and Machida, Y. (2002). ACR4, a putative receptor kinase gene of Arabidopsis thaliana, that is expressed in the outer cell layers of embryos and plants, is involved in proper embryogenesis. Plant Cell Physiol. *43*, 419–428.
40. Curtis, M.D., and Grossniklaus, U. (2003). A gateway cloning vector set for high-throughput functional analysis of genes in planta. Plant Physiol. *133*, 462–469.
41. Atanassov, I.I., Atanassov, I.I., Etchells, J.P., and Turner, S.R. (2009). A simple, flexible and efficient PCR-fusion/Gateway cloning procedure for gene fusion, site-directed mutagenesis, short sequence insertion and domain deletions and swaps. Plant Methods *5*, 14.
42. Schatlowski, N., Stahl, Y., Hohenstatt, M.L., Goodrich, J., and Schubert, D. (2010). The CURLY LEAF interacting protein BLISTER controls expression of polycomb-group target genes and cellular differentiation of Arabidopsis thaliana. Plant Cell *22*, 2291–2305.
43. Truernit, E., Bauby, H., Dubreucq, B., Grandjean, O., Runions, J., Barthélémy, J., and Palauqui, J.-C. (2008). High-resolution whole-mount imaging of three-dimensional tissue organization and gene expression enables the study of Phloem development and structure in Arabidopsis. Plant Cell *20*, 1494–1503.
44. Kudryavtsev, V., Felekyan, S., Woźniak, A.K., König, M., Sandhagen, C., Kühnemuth, R., Seidel, C.A.M., and Oesterhelt, F. (2007). Monitoring dynamic systems with multiparameter fluorescence imaging. Anal. Bioanal. Chem. *387*, 71–82.
45. Widengren, J., Kudryavtsev, V., Antonik, M., Berger, S., Gerken, M., and Seidel, C.A.M. (2006). Single-molecule detection and identification of multiple species by multiparameter fluorescence detection. Anal. Chem. *78*, 2039–2050.
46. Suhling, K., Siegel, J., Phillips, D., French, P.M.W., Lévêque-Fort, S., Webb, S.E.D., and Davis, D.M. (2002). Imaging the environment of green fluorescent protein. Biophys. J. *83*, 3589–3595.
47. Koshioka, M., Sasaki, K., and Masuhara, H. (1995). Time-dependent fluorescence depolarization analysis in three-dimensional microspectroscopy. Appl. Spectrosc. *49*, 224–228.
48. Schaffer, J., Volkmer, A., Eggeling, C., Subramaniam, V., Striker, G., and Seidel, C.A.M. (1999). Identification of Single Molecules in Aqueous Solution by Time-Resolved Fluorescence. J. Phys. Chem. A *103*, 331–336.
49. Becker, W. (2005). Advanced Time-Correlated Single Photon Counting Techniques (Berlin: Springer).